Mol Cell Biochem (2013) 372:199–210
DOI 10.1007/s11010-012-1461-1

Serum protein *N*-glycan alterations of diethylnitrosamine-induced hepatocellular carcinoma mice and their evolution after inhibition of the placental growth factor

Bram Blomme · Femke Heindryckx · Jean Marie Stassen · Anja Geerts · Isabelle Colle · Hans Van Vlierberghe

Received: 8 May 2012 / Accepted: 14 September 2012 / Published online: 24 September 2012

Abstract Placental growth factor (PlGF) inhibition produced promising results in reducing tumor burden in a diethylnitrosamine (DEN)-induced mouse model for hepatocellular carcinoma (HCC). The aim of this study was to non-invasively assess the improved histology by performing a serum glycomic analysis. To elucidate the molecular mechanism underlying the observed glycomic effects, we investigated the transcription and expression of E26 transformation-specific sequence 1 (Ets-1), a transcription factor essential for the glycomic and angiogenic changes in malignant transformation, including its different phosphorylated forms that result from activation of the MAP kinase and a Ca^{2+}-dependent pathway. In addition, three Ets-1-dependent glycosyltransferase genes, *Mgat4a*, *Mgat4b*, and *Mgat5*, were also evaluated. HCC was induced in mice by weekly injections with DEN for 16, 20, 25, and 30 w. In the treatment study, mice were injected with DEN for 25 w and subsequently treated with PlGF antibodies (5D11D4) for 5 w. Finally, PlGF−/− mice were injected with DEN for 20, 25, and 30 w. Serum *N*-glycans were analyzed with DNA sequencer-assisted fluorophore-assisted capillary electrophoresis and compared with histology. Maximum altered *N*-glycan phenotype was reached after 20 w of DEN-injections, i.e., when the first neoplastic lesions started to appear. 5D11D4-treatment improved the glycomic phenotype in that 7 of the 11 altered glycans tended to normalize. The PlGF−/− mice also showed a normalization trend, although not to the same extent of the treatment group. Number of *Ets1*, *Mgat4a*, *Mgat4b*, and *Mgat5* transcripts increased considerably in DEN-injected mice, however, a non-significant decrease was observed after 5D11D4-treatment. On the protein level, 5D11D4-treatment had a prominent effect on the MAP kinase pathway with a significant p38 activation, yet independent of Ets-1 function.

Keywords Glycomics · Hepatocellular carcinoma · Diethylnitrosamine · c-ets-1 protein · Angiogenesis inhibitors

Introduction

Annually, more than 560,000 people are diagnosed with primary liver cancer (PLCs), and hepatocellular carcinoma (HCC) accounts for 85–90 % of all PLCs [1]. The factors determining the risk for HCC include age, male gender, and etiology of the underlying liver disease. In particular, cirrhosis is associated with a significant risk for HCC [2]. A liver biopsy is currently the gold standard to diagnose the cirrhotic state of the liver, despite the well-known limitations and complications [3].

To overcome these problems, a lot of research is ongoing to develop non-invasive alternatives for liver biopsy using molecular biology tools. Callewaert et al. [4] have developed a test based on the *N*-glycosylation of serum proteins that can be used to diagnose cirrhotic from non-cirrhotic patients with high sensitivity and specificity. Using the same glycomic technique, Lui et al. [5] were able

Electronic supplementary material The online version of this article (doi:10.1007/s11010-012-1461-1) contains supplementary material, which is available to authorized users.

B. Blomme (✉) · F. Heindryckx · A. Geerts · I. Colle · H. Van Vlierberghe
Department of Hepatology and Gastroenterology, Ghent University Hospital, 9000 Ghent, Belgium
e-mail: bram.blomme@ugent.be

J. M. Stassen
ThromboGenics NV, Leuven, Belgium

to distinct HCC patients from cirrhotic patients. In HCC patients, branched fucosylated tri-antennary glycans (NA3b) were increased, whereas bisecting *N*-acetylglucosamine (GlcNAc)-modified biantennary glycans (NA2FB) were decreased compared to cirrhotic patients. However, the latter test was developed in hepatitis B patients. Hepatitis B virus (HBV) is considered an oncovirus, and this can be attributed to one of the four proteins that originate from the HBV genome, the HBx-protein [6]. It was shown that the HBx-protein significantly up-regulates the expression of *N*-acetylglucosaminyltransferase III (GnT-III), the enzyme responsible for the bisecting GlcNAc modification [7]. During tumor development, expression of GnT-V, responsible for β1-6 branching to form multi-antennary glycans, is up-regulated in HCC nodules and this enzyme will compete with GnT-III for the same substrate (tri-mannose core) [8]. Therefore, using this technique, advanced HCC (more and larger HCC nodules producing more GnT-V) can be more readily differentiated from cirrhosis compared to early HCC stages. However, these results could not be reproduced in a MALDI-TOF study with a mixed HCC-population of hepatitis B and hepatitis C patients [9]. Surprisingly, two multi-antennary *N*-glycans were significantly decreased, and a bisecting GlcNAc-modified biantennary glycan was significantly increased in serum of HCC patients. These glycomic changes are typical for cirrhotic patients and were probably induced by the dominating cirrhotic liver in these HCC patients.

The transcription factor E26 transformation-specific sequence 1 (Ets-1) is a product of proto-oncogenes related to malignant transformation and metastasis. It plays an important role in the process of angiogenesis and glycosylation. In the context of glycosylation, the GnT-V enzyme is under the oncogenic control of Ets-1 [10, 11]. In the context of angiogenesis, Ets-binding motifs are found in the promoter/enhancer region of numerous genes that are important for angiogenesis. These include VEGFR-1 and -2, Tie-1 and -2 which are involved in the activation of endothelial cells and matrix metalloproteinases and VE-cadherin which are involved in endothelial cell migration and capillary formation [12, 13]. The transcriptional activity of Ets-1 is regulated by multi-site phosphorylation. It has been shown that Ras/MAP kinase signaling stimulates Ets-1 transactivational activity. Activation of this pathway leads to the phosphorylation of Thr38 and increases its interaction with other proteins including AP-1 and AML-1 [14]. In contrast, phosphorylation of Ets-1 by Ca^{2+}-signaling pathways (on Ser251, Ser270, Ser273, Ser282, and Ser285) has been reported to block DNA binding, thereby inhibiting Ets-1 transcriptional activity [15, 16].

Placental growth factor (PlGF) is a homolog of vascular endothelial growth factor (VEGF), and was originally isolated from the human placenta [17]. VEGF can bind to VEGFR-1 and VEGFR-2, whereas PlGF binds to neuropilines and VEGFR-1 which are up-regulated in disease. It was previously shown that the angiogenic activity of PlGF is restricted to pathologic conditions, without affecting healthy vessels [18]. Furthermore, promising results have been obtained by inhibiting PlGF in several solid tumors [18]. Treatment of HCC in diethylnitrosamine (DEN)-induced mice with PlGF antibodies causes a substantial improvement in mortality, tumor burden, vascular normalization and arterialization, compared to the control group [19].

The variation of glycosylation is closely related to oncogenic transformation [20]. Therefore, profiling of glycans could be a promising strategy to non-invasively evaluate the efficacy of 5D11D4, a murine anti-PlGF monoclonal antibody, on tumor growth in DEN-induced HCC.

Materials and methods

Animals

5-week-old male WT (129S2/SvPasCrl) mice received weekly intraperiteoneal (IP) injections with DEN (35 mg/kg) (Sigma-Aldrich, St Louis, MO, USA). Mice were kept under constant temperature and humidity in a 12 h controlled light/dark cycle and received food and water ad libitum. The Ethical committee of experimental animals at the faculty of Medicine and Health Sciences, Ghent University, Belgium, approved the protocols [21].

WT mice injected with DEN were sacrificed after 16 w ($n = 5$), 20 w ($n = 11$), 25 w ($n = 10$), and 30 w ($n = 10$). WT control mice were injected with saline solution ($n = 10$). In the treatment study, WT mice were injected with DEN and control mice were injected with saline solution for 25 w and subsequently treated with 5D11D4 (25 mg/kg, 2×/week IP), a murine anti-PlGF monoclonal antibody, for 5 w ($n = 9$) or IgG for 5 w ($n = 9$). PlGF−/− mice injected with DEN were killed after 20 w ($n = 9$), 25 w ($n = 7$), and 30 w ($n = 5$). PlGF−/− control mice were injected with saline solution ($n = 6$).

At time of killing, blood was collected from the carotid artery under isoflurane (Forene®, Abbott, Brussels, Belgium) anesthesia. These samples were centrifuged at 2,000 rpm for 10 min. Serum was taken off the clot and stored at −80 °C for glycomic analysis. The right lobe of the liver in control mice, and the lobe with HCC nodules in DEN-treated mice were removed and fixed in 4 % phosphate-buffered formaldehyde solution for 24 h (Klinipath, Geel, Belgium).

N-glycan analysis

The *N*-glycans present in 3 μl of serum were released from the proteins with PNGase F, subsequently desialylated and fluorescently labeled with APTS. Improved DNA sequencer-assisted fluorophore-assisted capillary electrophoresis (DSA-FACE) technology was used to profile and analyze the labeled glycans [22]. Data were analyzed using the Genemapper v3.7 software (Applied Biosystems, Carlsbad, CA, USA). Thirteen peaks were present in the electropherogram of every mouse serum sample. The peak height of every peak was quantified to obtain a numerical description of the profiles. The peak heights were subsequently normalized to the total intensity of the measured peaks (represented as a percentage of the total peak height). Structural analysis of the *N*-glycans was done as previously described [23] (see Supplementary Fig. 1 for exoglycosidase digests). Based on these analyses, the following peaks could be deduced in the mouse total serum electropherogram: peak 1 is an agalacto, core-α-1,6-fucosylated biantennary (NGA2F), peak 5 is a bigalacto, biantennary glycan (NA2), peak 7 is a bigalacto, core-α-1,6-fucosylated biantennary glycan (NA2F), and peak 11 is a tri-antennary glycan (NA3). From the latter structure, it could be deduced that peaks 12 and 13 are also multi-antennary glycans. The remaining peaks could not be definitively determined.

RNA extraction and quantitative real-time PCR

RNA was extracted from frozen liver tissue of four control mice and from HCC and non-HCC frozen liver tissue of four DEN-injected (30 w) and four 5D11D4-treated mice (25 w DEN + 5 w 5D11D4) with Qiagen RNeasy mini kit according to the manufacturer's instructions (Qiagen, Westburg BV, The Netherlands) with on-column DNAse treatment (Qiagen). Needle homogenization was performed. Total RNA was quantified using spectrophotometry (Nanodrop; Thermo Scientific, Wilmington, DE, USA) and ranged from 448 ng to 35 μg with an average of 16.8 μg. cDNA was synthesized starting from 2 μg of total RNA by using iScript cDNA Synthesis Kit (Bio-Rad Laboratories Inc., Hercules, CA, USA).

PCR amplification reactions were carried out in a total volume of 8 μl containing 2× SYBR Green I Master Mix (Eurogentec, Seraing, Belgium), 3 μl 1/100 cDNA (~3.75 ng) and 250 nM forward and reverse primers (BioLegio, Nijmegen, The Netherlands). All reactions were performed in a 384-well plate (LightCycler 480 Multiwell Plates 384, white and LightCycler 480 Sealing Foils from Roche Diagnostics, Indianapolis, IN, USA) on the CFX384 real-time PCR detection system (Bio-Rad, Hercules, CA, USA), followed by a regression Cq value determination method. Cycling conditions were as follows: 95 °C for 10 min followed by 45 cycles of 95 °C for 10 s and 60 °C for 30 s, followed by a dissociation curve analysis from 60 to 95 °C. Primers containing neither SNPs nor secondary structures were designed for Glyceraldehyde 3-phosphate dehydrogenase (*Gapdh*), Succinate dehydrogenase complex subunit A (*Sdha*), *Ets1*, *Mgat4a*, *Mgat4b*, and *Mgat5* (Table 1). BLAST searches confirmed that only the target genes were 100 % covered. A 6-point fourfold standard dilution series (highest concentration; 32 ng/μl) of a cDNA mixture of all samples included in the study diluted in 5 ng/μl tRNA (Roche) was used to test the PCR efficiency of the primers. The mRNA expression level of each gene was determined in Excel by using the comparative 2-(delta delta Cq) method and normalized to the geometric mean of the stably expressed reference genes *Gapdh* and *Sdha*.

Western blot analysis of MAP kinase and Ca^{2+}-dependent pathways

HCC-lesions and non-HCC-tissue of five DEN-injected (30 w) and five 5D11D4-treated (25 w DEN + 5 w 5D11D4) mice were separately collected and snap frozen in liquid nitrogen. Liver tissue of one control sample was also included in the analysis. The snap-frozen tissues were lysed in radioimmunoprecipitation assay buffer (25 mmol/l Tris, 50 mmol/l NaCl, 0.5 % NP40, 0.5 % deoxycholate, 0.1 % SDS, 0.0555 g/ml β-glycerophosphate, 1 mmol/l DTT, phosphatase inhibitor cocktail, and mini-EDTA-free protease inhibitor) by sonication in an ice bath. Total protein content was determined with the Bio-Rad DC protein assay kit (Bio-Rad, Hercules, CA, USA), and absorbance was measured on a plate reader at 590 nm.

One hundred micrograms of protein per lane was mixed with LDS sample buffer (Nupage; Invitrogen, Seattle, WA,

Table 1 Sequence of PCR primers, PCR efficiencies (%), and correlation coefficients (R^2)

Gene symbol	Forward primer	Reverse primer	PCR efficiency	R^2
Sdha	CTTGAATGAGGCTGACTGTG	ATCACATAAGCTGGTCCTGT	102.8	0.9924
Gapdh	CATGGCCTTCCGTGTTCCTA	GCGGCACGTCAGATCCA	87.47	0.9999
Ets1	GCTCAGTGTGTTCCTCCCTC	GATGCAGCGTCTGATAGGACT	94.33	0.999
Mgat4a	ATGAGGCTCCGAAATGGAACT	CCACTCGAAGACGCTCTTTTAG	94.04	0.99
Mgat4b	GAAGCCGTGGAACGTCTCG	GTACGCTCGGAATGCCCAT	100.2	0.99
Mgat5	AAGGTGGACAATCTGGTCAACG	GCCATCCATAGGAGGCAATAC	96.9	0.97

USA) and a sample reducing agent (dithiothreitol, Invitrogen). The proteins were denatured by heating at 70 °C for 10 min, subsequently loaded onto 10 % Bis–Tris gel (Invitrogen), separated, and transferred to a nitrocellulose membrane (GE Healthcare, Little Chalfont, Buckinghamshire, United Kingdom). Membranes were blocked in Tris-buffered saline containing 0.05 % Tween and 5 % non-fat milk (TBST/5 % milk). Blots were probed overnight at 4 °C with antibodies directed against the non-phosphorylated and phosphorylated forms of ERK1/2, JNK, and p38 (MAP kinase pathway) (Cell Signaling Technology, Beverly, MA, USA) and the phosphorylated forms of PKC-alpha and CaMKII (Ca^{2+}-dependent pathway) (Life Technologies Ltd, Paisley, UK and Cell Signaling Technology, Beverly, MA, USA, respectively). Expression of the Ets-1 protein and its different phosphorylated forms were investigated by probing blots overnight at 4 °C with antibodies directed against the non-phosphorylated form (Santa Cruz Biotechnology, Santa Cruz, CA, USA), the Thr38-phosphorylated form, the Ser251-phosphorylated form and the Ser282/285 double-phosphorylated form (MBL International, Woburn, MA, USA). The dilution used in all blots was 1:1,000. After three washes with TBST, the membranes were incubated for 1 h with secondary antibodies (Cell Signaling, Beverly, MA, USA; dilution 1:2,000). Horseradish peroxidase detection was carried out with an enhanced chemiluminescence substrate (Roche Diagnostics, Indianapolis, IN, USA). Blots were subsequently stripped and reprobed with monoclonal antibodies against actin (Abcam, Cambridge, UK; dilution 1:400) as an internal control for protein loading. ImageJ software (National Institutes of Health, Bethesda, MD; http://rsb.info.nih.gov/ij/) was used to quantify western blot signals.

Statistical analysis

Statistical analysis was performed with SPSS 19.0 (SPSS, Chicago, IL, USA). For the glycomic analysis, all time points (16, 20, 25, and 30 w of DEN) were compared to control mice (DEN-study). Subsequently, 25 w of DEN-injections and 5 w of 5D11D4-treatment were compared to mice that were injected with DEN for 25 w followed by 5 w of control IgG (treatment study). Finally, all time points of DEN-injected PlGF−/− mice (20, 25, and 30 w) were compared to control PlGF−/− mice. In addition, DEN-injected PlGF−/− mice were compared to the concordant DEN-injected WT mice (PlGF−/− study).

For the qPCR analysis, three groups were compared to each other in HCC and non-HCC tissue (30 w of DEN vs. control, 30 w of DEN vs. 5D11D4-treated and 5D11D4-treated vs. control). Finally, western blot data were analyzed DEN-injected vs. 5D11D4-treated in HCC and non-HCC-tissue. Glycomic, qPCR, and western blot data were processed using a non-parametric Mann–Whitney U test. P values <0.05 were considered significant in all analyses.

Results

Histological analysis

After 16 weeks of weekly DEN-injections, a mild fibrosis occurs and dysplastic lesions start to appear, resulting in a premalignant environment. The following weeks are a

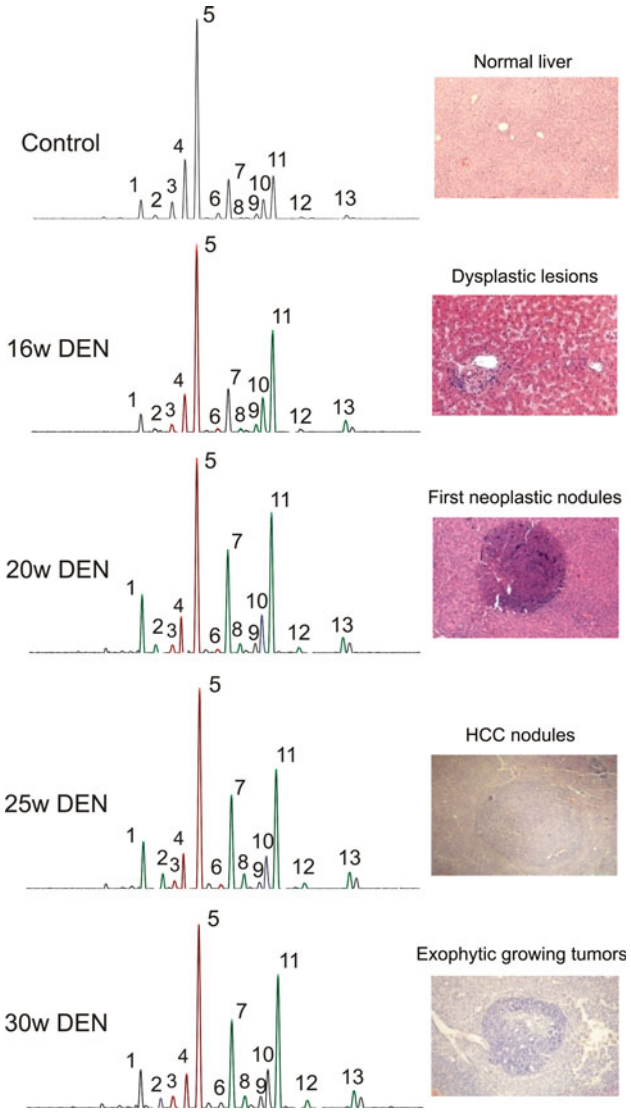

Fig. 1 *N*-glycomic analysis of serum proteins in control and DEN-injected mice. Representative serum *N*-glycosylation patterns of control wild-type mice and wild-type mice chronically injected with DEN for 16, 20, 25, and 30 w. A representative histological slide for each time point (stained hematoxylin–eosin) is presented next to the concordant *N*-glycan profile. *Green* significantly increased in relative peak height compared to control mice; *red* significantly decreased in relative peak height compared to control mice. (Color figure online)

Table 2 *N*-glycomic analysis in the DEN-study, treatment study, and PlGF−/− study

Study	Time point	Peak 1	Peak 2	Peak 3	Peak 4	Peak 5	Peak 6	Peak 7	Peak 8	Peak 9	Peak 10	Peak 11	Peak 12	Peak 13
DEN[a]	16 w			↓*	↓**	↓**	↓**		↑**	↑*	↑**	↑**		↑**
	20 w	↑***	↑*	↓**	↓***	↓***	↓**	↑***	↑***			↑***	↑*	↑***
	25 w	↑**	↑**	↓**	↓***	↓***	↓**	↑***	↑***			↑***	↑*	↑***
	30 w			↓*	↓***	↓***		↑***	↑***			↑**	↑***	↑***
Treatment[b]	5 w 5D11D4		↓*	↑**	↑*				↓*			↓**	↓*	↓**
PlGF−/−[c]	20 w	↑**			↓***	↓***	↓***		↑***	↑**	↑***	↑***	↑**	↑*
	25 w	↑*	↑*		↓**	↓**	↓**		↑**	↑**	↑**	↑**	↑**	↑**
	30 w				↓**	↓**		↑**	↑**	↑*		↑*	↑**	↑**
PlGF−/−[d]	Control			↓**		↑*				↓***	↓***			↓**
	20 w				↑*	↑**		↓***	↓***					↓**
	25 w				↑**	↑*		↓***	↓**					↓***
	30 w	↑*				↑*					↓**	↓**		↓*

↓, Significantly decreased in abundance; ↑, significantly increased in abundance

* $P < 0.05$; ** $P < 0.01$; *** $P < 0.001$

[a] Compared to control mice;

[b] Compared to 25 w DEN and 5 w IgG

[c] Compared to control PlGF−/− mice

[d] Compared to the corresponding WT mice

progression phase in which the premalignant environment continues to evolve to a malignant state. The tumor burden significantly augments and angiogenic factors persist to increase. After 25 w of DEN-injections, the small dysplastic lesions have progressed to vascularized exophytically growing tumors which are macroscopically visible and give rise to a further increase in angiogenic factors, leading to the formation of new blood vessels. Histologically, tumor burden reached a maximum phenotype after 30 w of DEN-injections that was significantly larger compared to 25 w. Inhibition of PlGF in this model, leads to a decreased tumor burden, vascular normalization, decreased arterializations, and a prolonged survival compared to DEN-induced controls [21].

N-glycomic analysis

DEN-study

After 16 w of DEN, 9 of the 13 peaks in the electropherogram were significantly altered in comparison to control mice. Maximum altered phenotype on the *N*-glycomic level (11 of the 13 peaks) was reached after 20 w of DEN, and this is also the time point when small neoplastic lesions started to appear. After 30 w of DEN, all mice have developed well-vascularized, macroscopic lesions, although the glycomic phenotype did not further aggravate in comparison to 20 w (and 25 w) of DEN; even a slight reduction in severity of the glycomic phenotype was observed (Fig. 1) (for *P* values, see Table 2).

Treatment study

We compared the serum *N*-glycosylation patterns of mice injected with DEN for 25 w and subsequently treated with 5D11D4 for 5 w with the serum *N*-glycosylation patterns of mice injected with DEN for 25 w and treated with control IgG for 5 w. The latter group showed the same alterations (including a supplementary significant increase of peak 12) compared to 25 w DEN alone indicating that IgG treatment did not influence the glycomic phenotype.

Seven of the 11 altered peaks, observed after 25 w of DEN and 5 w of IgG, evolved back into the normal direction after 5 w treatment with 5D11D4, i.e., they significantly increased or decreased in peak height into the direction observed in control mice (Fig. 2) (for *P* values, see Table 2). We especially observed a normalization trend for all the multiantennary *N*-glycans (peaks 11, 12, and 13).

We also compared the serum *N*-glycosylation patterns of WT mice injected with saline solution for 25 w and subsequently treated with 5D11D4 with those of control mice. None of the 13 peaks were significantly altered in peak height compared to control mice indicating that 5D11D4 on itself had no effect on the serum *N*-glycosylation patterns (Fig. 2).

PlGF−/− study

We first compared control PlGF−/− mice with the different time points of DEN-injected PlGF−/− mice.

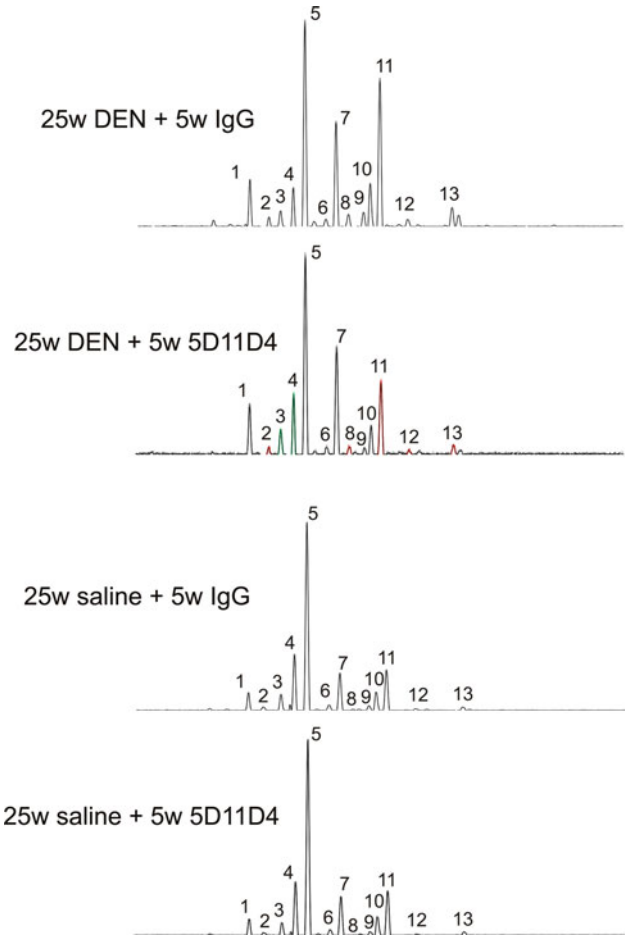

Fig. 2 *N*-glycomic analysis of serum proteins in DEN and saline-injected mice treated with IgG or 5D11D4. Representative serum *N*-glycosylation patterns of wild-type mice chronically injected with DEN or saline for 25 w and subsequently treated with IgG for 5 w and wild-type mice chronically injected with DEN or saline for 25 w and subsequently treated with 5D11D4 for 5 w. *Green* significantly increased in relative peak height compared to control IgG; *red* significantly decreased in relative peak height compared to control IgG. (Color figure online)

Maximum altered glycomic phenotype was observed after 25 w in which 11 of the 13 peaks were significantly altered. Similar to the DEN-study, the 30 w time point showed a reduction in severity of glycomic profile. Moreover, the altered peaks were also very consistent over the different time points with a significant decrease of peaks 4 and 5 and a significant increase of peaks 8, 9, 11, 12, and 13. After 20 and 25 w, there was a supplementary significant increase of peaks 1 and 10 and a significant decrease of peak 6. Peak 2 was only significantly increased after 25 w, and peak 7 was only significantly increased after 30 w (for *P* values, see Table 2).

Subsequently, we compared control and DEN-injected PlGF−/− mice with their WT counterpart. Interestingly, already at baseline (control PlGF−/− vs. control WT), five peaks were significantly altered. A significant increase of peak 5 and a significant decrease of peaks 3, 9, 10, and 13 were observed (Fig. 3a). After 20 and 25 w, the PlGF−/− displayed a significant increase of peaks 4 and 5 and a significant decrease of peaks 7, 8 and 13. After 30 w, the glycomic profile somewhat differed with a significant increase of peaks 1 and 5 and a significant decrease of peaks 10, 11, and 13 (Fig. 3b) (for *P* values, see Table 2).

Fig. 3 *N*-glycomic analysis of serum proteins in WT and PlGF−/− mice. **a** Representative serum *N*-glycosylation pattern of control wild-type mice and control PlGF−/− mice. **b** Representative serum *N*-glycosylation patterns of WT and PlGF−/− mice injected with DEN for 20, 25, and 30 w. *Green* significantly increased in relative peak height compared to control mice; *red* significantly decreased in relative peak height compared to control mice. (Color figure online) ▶

Transcriptional levels of *Ets1*, *Mgat4a*, *Mgat4b*, *and Mgat5* in control, DEN-injected, and 5D11D4-treated mice

Quantitative evaluation of *Ets1* mRNA in DEN-injected mice revealed an increase of 1.94-fold surrounding the tumor and 3.02-fold in the tumor compared to control mice ($P = 0.2$ and $P = 0.057$, respectively). 5D11D4-treatment resulted in a 18.8 % reduction of *Ets1* mRNA transcripts surrounding the tumor and a 17.7 % reduction of *Ets1* mRNA transcripts in the tumor ($P = 0.686$ and $P = 0.886$, respectively, DEN-injected vs. 5D11D4-treated). However, these 5D11D4-treated samples still showed a 1.64-fold induction surrounding the tumor and 2.57-fold induction in the tumor when compared to control mice ($P = 0.343$ and $P = 0.114$, respectively).

The pattern of transcriptional level for *Mgat4a*, *Mgat4b*, and *Mgat5* in the different treatment groups was similar to that observed for *Ets1* (Fig. 4a). However, the fold increase in DEN-injected mice was considerably larger for the glycosyltransferase genes, especially *Mgat5*. A fold increase of 4.91 surrounding the tumor and a fold increase of 7.42 in the tumor was observed for *Mgat4a*, a fold increase of 3.78 surrounding the tumor and a fold increase of 7.07 in the tumor was observed for *Mgat4b* and, finally, a fold increase of 12.25 surrounding the tumor and a fold increase of 22.21 in the tumor was observed for *Mgat5*.

These results were linked to the observation that glycosyltransferase mRNA levels were below detection limit in the majority of control mice indicating their low abundant expression under normal circumstances. Consequently, we did not perform statistical analyses between control mice and DEN-injected mice and between control mice and 5D11D4-treated mice, but it was apparent that transcription of *Mgat4b* and *Mgat5* was considerably increased in DEN-injected mice and this still was the case after 5D11D4-treatment, both surrounding and in the tumor. Although *Mgat4a* had a similar pattern of transcription, mRNA levels

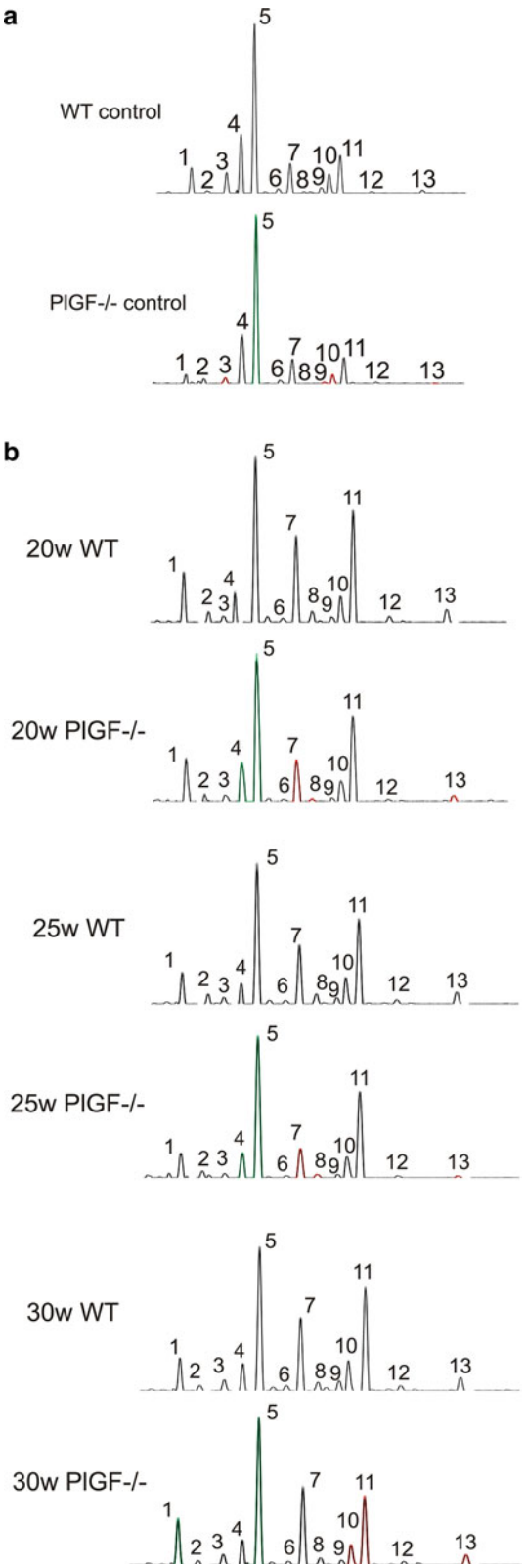

were overall very low, even in DEN-injected mice. For the *Mgat4b* gene, 5D11D4-treatment resulted in a 28.4 % reduction of mRNA transcripts surrounding the tumor and a 23.6 % reduction of mRNA transcripts in the tumor ($P = 0.486$ and $P = 0.686$, respectively). For the *Mgat5* gene, 5D11D4-treatment resulted in a 36.1 % reduction of mRNA transcripts surrounding the tumor and a 39.6 % reduction of mRNA transcripts in the tumor ($P = 0.886$ and $P = 0.343$, respectively).

Protein analysis of MAP kinase and Ca^{2+}-dependent signaling pathways

First, the non-phosphorylated forms of the MAP kinase pathway were investigated surrounding and in the tumor. A significant increased concentration of ERK1/2 was observed surrounding the tumor ($P = 0.028$) and, in contrast, a significant decreased concentration of JNK was observed in the tumor of 5D11D4-treated mice ($P = 0.008$). Analysis of the phosphorylated forms showed a strong activation of p38 following 5D11D4-treatment in both tissue types ($P = 0.008$ for both analyses). There was also a trend for the activation of ERK1/2 surrounding and in the tumor ($P = 0.095$ and $P = 0.16$, respectively) (Fig. 4b).

Subsequently, we investigated the phosphorylated forms of PKC-alpha and CaMKII. Surrounding the tumor, activated PKC-alpha expression was barely detected and the normalized concentration of CaMKII was similar in DEN-injected and 5D11D4-treated mice ($P = 0.69$). In the tumor, signal intensity of activated PKC-alpha and CaMKII was also alike in both groups ($P = 1.0$ and $P = 0.548$, respectively) (Fig. 4c).

Protein analysis of Ets-1 and its phosphorylated forms

Ets-1 showed a significant increase surrounding the tumor in its non-phosphorylated form ($P = 0.009$), whereas no such increase was found in the tumor of 5D11D4-treated mice ($P = 0.841$) (Fig. 4d). The Thr38 phosphorylated form, downstream of the MAP kinase pathway, did not show a significant alteration, both in and surrounding HCC-lesions ($P = 0.841$ and $P = 0.151$, respectively). Similary, the pSer251 phosphorylated and pSer282/285 double-phosphorylated form, downstream of the Ca^{2+}-dependent pathway, were not significantly different in and surrounding HCC-lesions ($P = 0.69/0.421$ and $P = 0.222/0.841$, respectively) (Fig. 4d).

Discussion

Mouse models of chronic liver disease produce large quantitative alterations of serum *N*-glycans. We did not only observe this in fibrotic models such as CCl_4 or common bile duct ligation [24], but also in this DEN-induced HCC-model virtually all serum *N*-glycans were

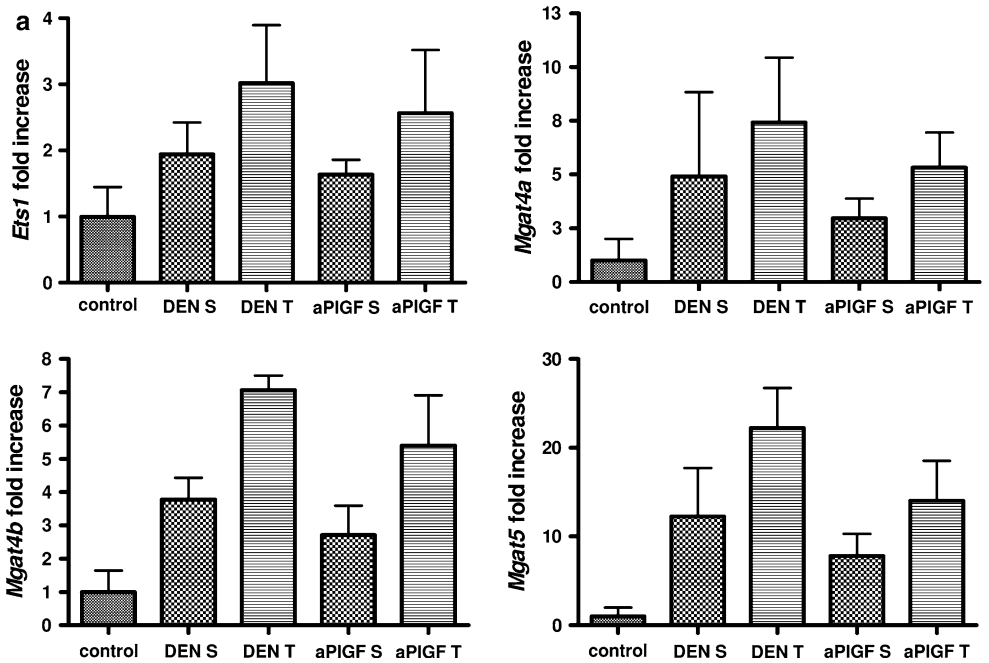

Fig. 4 Transcriptional and protein expression analysis of Ets-1. **a** Transcriptional analysis of *Ets1*, *Mgat4a*, *Mgat4b*, and *Mgat5*. Levels in control mice were arbitrary set as 1, and levels in DEN-injected mice surrounding (DEN S) and in the tumor (DEN T) as well as treated with 5D11D4 for 5 w surrounding (aPlGF S) and in the tumor (aPlGF T) expressed as the ratio to healthy controls. **b**–**d** Protein expression analysis of Ets-1 and its different phosphorylated forms that result from activation of the MAP kinase and Ca^{2+}-dependent pathway. Immunoblotting on liver tissue surrounding the tumor (S) and in the tumor (T) of 1 control mouse, three mice injected with DEN for 30 w (30 w DEN) and three mice injected with DEN for 25 w and subsequently treated with 5D11D4 for 5 w (5D11D4). **b** Signal intensity of non-phosphorylated and phosphorylated forms of ERK1/2, JNK and p38 (MAP kinase pathway). **c** Signal intensity of phosphorylated forms of PKC-α and CaMKII (Ca^{2+}-dependent pathway). **d** Signal intensity of non-phosphorylated Ets-1 and phosphorylated form pThr38, pSer251, and pSer282/285. Quantitative data of each western blot is provided. *Error bars* indicate SD. * $P < 0.05$; ** $P < 0.01$

significantly altered in abundance. This can be explained by the liver specificity of *N*-glycan alterations in mouse models of chronic liver disease [23]. In human liver disease, IgG is the main glycoprotein on which the glycomic changes occur [25, 26], but in mouse models of chronic liver disease, the impact of IgG *N*-glycosylation on total serum *N*-glycosylation is minimal, and the main alterations can be found on liver-produced proteins [23]. This was confirmed by a study similar to ours that also investigated *N*-glycomic changes in a DEN-induced HCC model [27]. They did not find any alteration of IgG glycan profiles in DEN-treated mice compared to controls.

In relation to HCC, Ets-1 has a different expression pattern in comparison to other neoplasms in which it is particularly enhanced in noncancerous lesions adjacent to HCC lesions [28]. This might explain the maximum altered *N*-glycomic phenotype occurring at an early stage of hepatocarcinogenesis. In this way, serum *N*-glycosylation pattern can be used as an early diagnostic tool for murine HCC.

In addition, the serum glycomic analysis performed by the DSA-FACE technology has several advantages for non-invasive murine and human testing. These include robustness, high throughput, high sensitivity, and reliable quantification. Furthermore, it is possible to routinely resolve isobaric glycan stereoisomers, which is much more difficult by mass spectrometry [22]. However, the preparatory steps to enable *N*-glycan analysis on capillary electrophoresis equipment are time-consuming. Moreover, these systems are expensive and are only found in the larger diagnostic molecular laboratories. These problems have recently been overcome with the development of a shortened protocol compatible with high-throughput-profiling in clinical chemistry laboratories [29].

Treatment with 5D11D4 produced a clear trend towards normalization on the *N*-glycomic level. However, the *N*-glycosylation patterns of the 5D11D4-treated mice were still significantly different from the *N*-glycan profiles of control mice. Anti-angiogenic therapy can prevent tumor growth and cause shrinkage by depriving tumors from their blood supply, yet a complete disappearance of tumor mass will not be accomplished. Interestingly, the PlGF−/− mice displayed less normalization of the glycomic phenotype compared to the 5D11D4-treatment group. This correlated with the histological data in which the effects on mortality, tumor size, and burden were less profound in the knock out

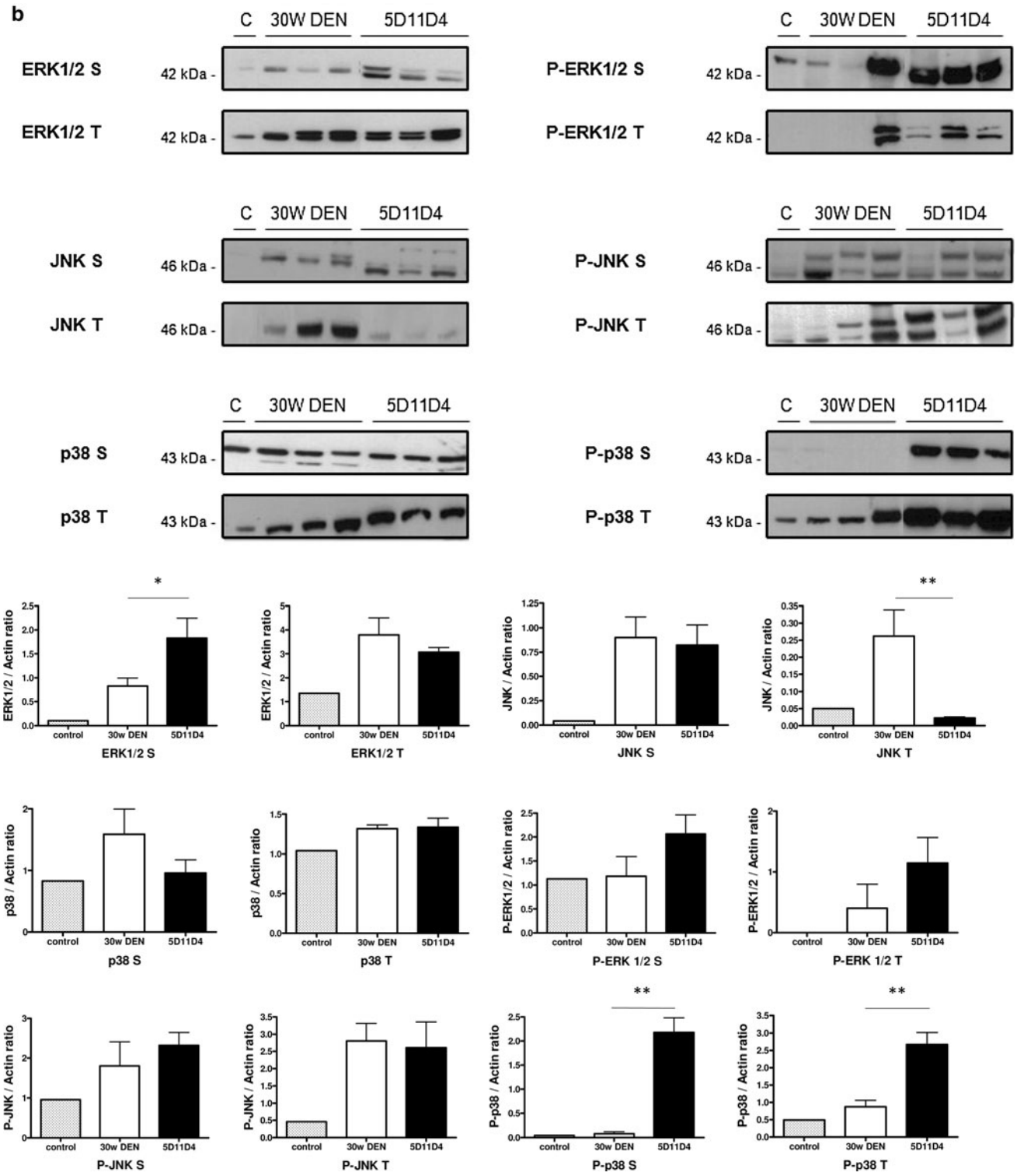

Fig. 4 continued

model than in the treatment study [19]. Tumors that occur in the knock out model have the chance to adapt to an environment without PlGF. Therefore, these tumors might have a different phenotype than those in WT mice.

The most elaborate changes after 5D11D4-treatment were observed in the multi-antennary *N*-glycan fraction with a strong decrease of all these glycans (peaks 11, 12, and 13). This drew our attention to the Ets-1 transcription

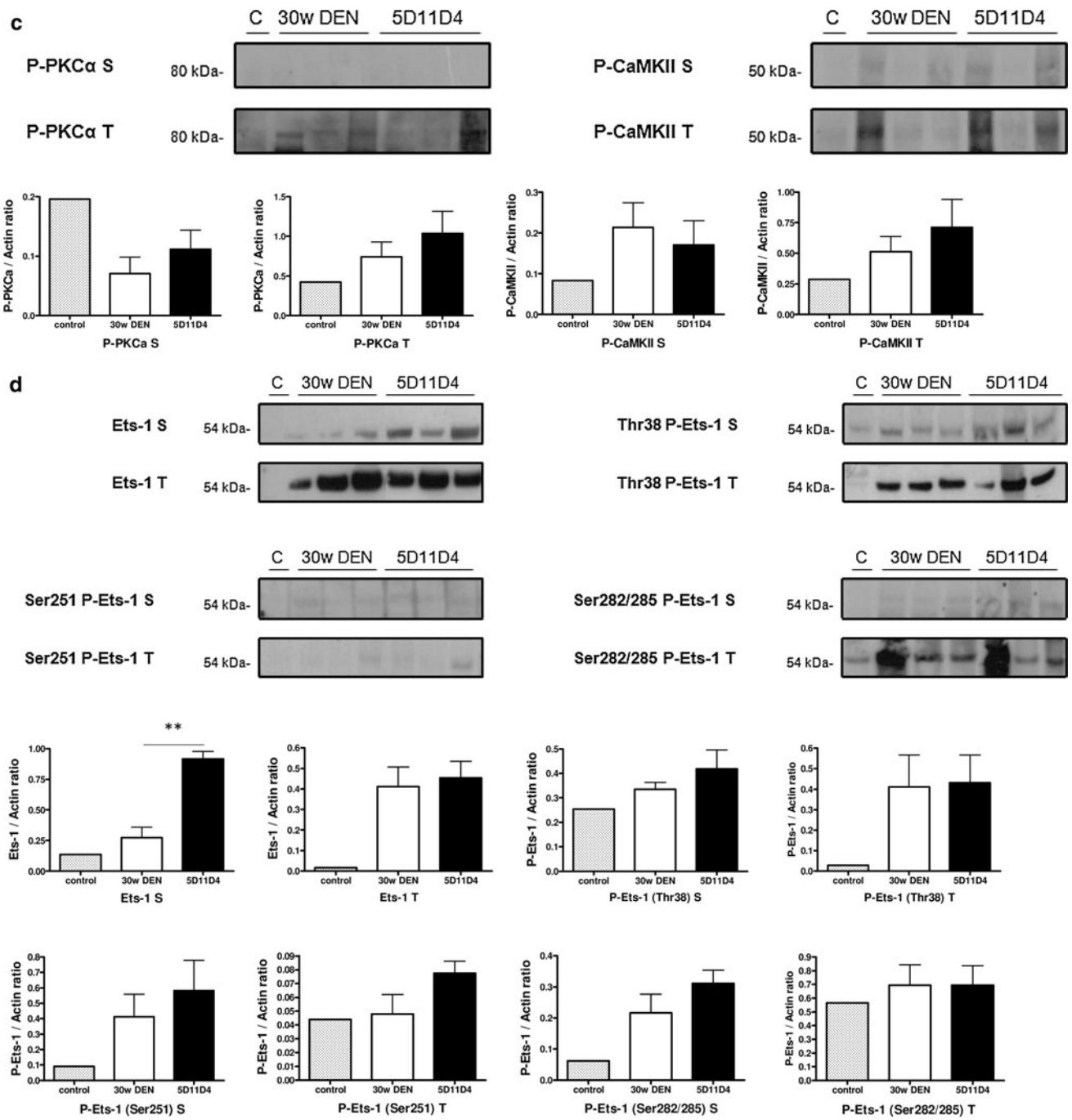

Fig. 4 continued

factor, essential for GnT-V expression in cancer cells, to investigate the molecular basis underlying the glycomic alterations. As expected, the number of *Ets1* transcripts doubled surrounding the tumor and tripled in the tumor. However, no relevant decrease in *Ets1* transcription was observed surrounding or in the tumor of 5D11D4-treated mice. In addition to oncogenic expression of GnT-V, Ets-1 is also involved in the transcription of GnT-IV, which has two isoenzymes, GnT-IVa and GnT-IVb. They both initiate the GlcNAcβ1-4 branch on the Manα1-3 arm of the *N*-glycan core and, together with GnT-V, they increase and preserve *N*-glycan branch complexity [30]. Even in DEN-injected mice, transcriptional level of *Mgat4a* barely rose above the detection limit suggesting its limited contribution to the alterations observed in the multi-antennary *N*-glycomic fraction. In contrast, transcriptional levels of *Mgat4b* and *Mgat5* were strongly and relevantly increased following 30 w of DEN-injections. The importance of *Mgat5* in

oncogenic development and cancer progression is well-established and our study additionally indicated an important role for *Mgat4b* in this process. As expected, no significant decrease in transcription of these glycosyltransferase genes was observed surrounding or in the tumor of 5D11D4-treated mice.

On the protein level, non-phosphorylated Ets-1 was quantified by WB analysis and showed a significant increase surrounding the tumor in 5D11D4-treated mice compared to DEN-injected mice, whereas no significant difference could be found in the tumor. Subsequently, the MAP kinase pathway was studied. The importance of this pathway in controlling cellular responses to the environment and in regulating gene expression, cell growth and apoptosis made it first choice to explore. We showed that 5D11D4-treatment had a prominent effect on this pathway with an activation of two well-characterized subfamilies of MAP kinases, p38 and ERK, but not JNK. The most elaborate activation was observed for p38, showing no difference in its non-phosphorylated form, but a strong up-regulation in HCC and non-HCC tissue following 5D11D4-treatment. A large amount of literature supports the role for p38 as suppressor of tumorigenesis [31–33]. In the context of HCC, p38 activation negatively regulates tumorigenesis by antagonizing the JNK-c-Jun pathway which is confirmed by our findings in this DEN-induced HCC mouse model [34]. In addition, p38 has opposing effects on endothelial cells in which activation of p38 inhibits cell proliferation and induces cell migration. Therefore, prolonged activation of p38 may result in an anti-angiogenic phenotype that contributes to endothelial dysfunction such as an increased endothelial cell permeability [35, 36]. However, loss of PlGF was shown to protect mice against vascular leakage [37] indicating that our data predominantly reflects (pre-)malignant hepatocyte tissue.

The phosphorylated forms of Ets-1 did not offer an explanation for the observed phenotype. A significant increase of pThr38-Ets-1 was not observed, neither surrounding the tumor, nor in the tumor. We, therefore, suggest that Ets-1 phosphorylation by the MAP kinase pathway has no influence on DNA binding thereby confirming results obtained by others [15, 38]. In addition, the phosphorylated forms upstream (PKC-alpha and CaMKII) and downstream the Ca^{2+}-dependent pathway (pSer251 and pSer282/285) showed no significant difference in and surrounding the tumor of DEN-injected and 5D11D4-treated mice. To sum up, Ets-1 explained the increase of multi-antennary glycans in the DEN-induced HCC model, but it did not provide evidence for the down-regulation of this glycomic fraction following PlGF inhibition. This suggested that the diminished tumor size caused by PlGF inhibition was sufficient for the observed normalization of glycomic phenotype. This was reinforced by the macroscopic data of 5D11D4-treated and PlGF−/− mice that reflected the different quantitative normalization of the glycomic profile.

In conclusion, maximum altered phenotype on the glycomic level was reached at an early stage of carcinogenesis and treatment with anti-PlGF monoclonal antibodies significantly improved the majority of the altered *N*-glycans, whereas PlGF−/− mice showed less glycomic normalization. We also showed that 5D11D4-treatment had a prominent effect on the MAP kinase pathway with especially a strong activation of p38 in tumoral and non-tumoral tissue independent of Ets-1 function.

Acknowledgments BB receives a scholarship GOA BOFF07/GOA/017 of the University Ghent Research Fund (BOF). HVV is Senior Clinical Investigator of the Research Foundation (FWO). FH is funded by a FWO grant (Aspirant FWO, FWO09/ASP/161).

Conflict of interest JM Stassen is a shareholder and Head of preclinical R&D of ThromboGenics NV and named in a patent related to data reported in this article which may result in payment of royalties. The other authors declare no conflict of interest.

References

1. Nordenstedt H, White DL, El-Serag HB (2010) The changing pattern of epidemiology in Hepatocellular carcinoma. Dig Liver Dis 42(Suppl 3):S206–S214
2. Sherman M (2005) Hepatocellular carcinoma: epidemiology, risk factors, and screening. Semin Liver Dis 25:143–154
3. Piccinino F, Sagnelli E, Pasquale G, Giusti G (1986) Complications following percutaneous liver biopsy. A multicentre retrospective study on 68,276 biopsies. J Hepatol 2:165–173
4. Callewaert N, Van Vlierberghe H, Van Hecke A, Laroy W, Delanghe J, Contreras R (2004) Noninvasive diagnosis of liver cirrhosis using DNA sequencer-based total serum protein glycomics. Nat Med 10:429–434
5. Liu XE, Desmyter L, Gao CF et al (2007) N-glycomic changes in hepatocellular carcinoma patients with liver cirrhosis induced by hepatitis B virus. Hepatology 46:1426–1435
6. Xu J, Yun X, Jiang J et al (2010) Hepatitis B virus X protein blunts senescence-like growth arrest of human hepatocellular carcinoma by reducing Notch1 cleavage. Hepatology 52:142–154
7. Shim JK, Lee YC, Chung TH, Kim CH (2004) Elevated expression of bisecting *N*-acetylglucosaminyltransferase-III gene in a human fetal hepatocyte cell line by hepatitis B virus. J Gastroenterol Hepatol 19:1374–1387
8. Yanagi M, Aoyagi Y, Suda T, Mita Y, Asakura H (2001) *N*-Acetylglucosaminyltransferase V as a possible aid for the evaluation of tumor invasiveness in patients with hepatocellular carcinoma. J Gastroenterol Hepatol 16:1282–1289
9. Goldman R, Ressom HW, Varghese RS et al (2009) Detection of hepatocellular carcinoma using glycomic analysis. Clin Cancer Res 15:1808–1813
10. Kang R, Saito H, Ihara Y et al (1996) Transcriptional regulation of the *N*-acetylglucosaminyltransferase V gene in human bile duct carcinoma cells (HuCC-T1) is mediated by Ets-1. J Biol Chem 271:26706–26712
11. Ko J, Miyoshi E, Noda K et al (1999) Regulation of the GnT-V promoter by transcription Ets-1 in various cancer cell lines. J Biol Chem 274:22941–22948

12. Sato Y (2001) Role of ETS family transcription factors in vascular development and angiogenesis. Cell Struct Funct 26:19–24
13. Wernert N, Raes MB, Lassalle P et al (1992) c-ets1 proto-oncogene is a transcription factor expressed in endothelial cells during tumor vascularization and other forms of angiogenesis in humans. Am J Pathol 140:119–127
14. Yang B, Hauser C, Henkel G et al (1996) Ras-mediated phosphorylation of a conserved threonine residue enhances the transactivation activities of c-Ets-1 and c-Ets-2. Moll Cell Biol 16:538–547
15. Cowley D, Graves B (2000) Phosphorylation represses Ets-1 DNA binding by reinforcing autoinhibition. Genes Dev 14: 366–376
16. Pufall M, Lee G, Nelson M et al (2005) Variable control of Ets-1 DNA binding by multiple phosphates in an unstructured region. Science 309:142–145
17. Maglione D, Guerriero V, Viglietto G, Dellibovi P, Persico M (1991) Isolation of a human placenta cDNA coding for a protein related to the vascular permeability factor. Proc Natl Acad Sci USA 88:9267–9271
18. Fischer C, Jonckx B, Mazzone M et al (2007) Anti-PlGF inhibits growth of VEGF(R)-inhibitor-resistant tumors without affecting healthy vessels. Cell 131:463–475
19. Van de Veire S, Stalmans I, Heindryckx F et al (2010) Further pharmacological and genetic evidence for the efficacy of PlGF inhibition in cancer and eye disease. Cell 141:178–190
20. Tang Z, Varghese R, Bekesova S et al (2010) Identification of *N*-glycan serum markers associated with hepatocellular carcinoma from mass spectrometry data. J Proteome Res 9:104–112
21. Heindryckx F, Mertens K, Charette N et al (2010) Kinetics of angiogenic changes in a new mouse model for hepatocellular carcinoma. Mol Cancer 9:219–232
22. Laroy W, Contreras R, Callewaert N (2006) Glycome mapping on DNA sequencing equipment. Nat Protoc 1:397–405
23. Blomme B, Van Steenkiste C, Callewaert N, Van Vlierberghe H (2011) Alterations of serum protein *N*-glycosylation in two models of chronic liver disease are hepatocyte and not B cell driven. Am J Physiol Gastrointest Liver Physiol 300:G833–G842
24. Blomme B, Van Steenkiste C, Vanhuysse J, Colle I, Callewaert N, Van Vlierberghe H (2010) Impact of elevation of total bilirubin level and etiology of the liver disease on serum *N*-glycosylation patterns in mice and humans. Am J Physiol Gastrointest Liver Physiol 298:G615–G624
25. Klein A, Carre Y, Louvet A, Michalski JC, Morelle W (2010) Immunoglobulins are the major glycoproteins involved in the modifications of total serum *N*-glycome in cirrhotic patients. Proteomics Clin Appl 4:379–393
26. Vanderschaeghe D, Laroy W, Sablon E et al (2009) GlycoFibroTest is a highly performant liver fibrosis biomarker derived from DNA sequencer-based serum protein glycomics. Mol Cell Proteomics 8:986–994
27. Liu XE, Dewaele S, Vanhooren V et al (2010) Alteration of *N*-glycome in diethylnitrosamine-induced hepatocellular carcinoma mice: a non-invasive monitoring tool for liver cancer. Liver Int 30:1221–1228
28. Ito Y, Miyoshi E, Takeda T et al (2000) Expression and possible role of ets-1 in hepatocellular carcinoma. Am J Clin Pathol 114:719–725
29. Vanderschaeghe D, Szekrényes A, Wenz C et al (2010) High-throughput profiling of the serum *N*-glycome on capillary electrophoresis microfluidics systems: towards clinical implication of the GlycoHepatoTest. Anal Chem 82:7408–7415
30. Takamatsu S, Antonopoulos A, Ohtsubo K et al (2010) Physiological and glycomic characterization of *N*-acetylglucosaminyltransferase-IVa and -IVb double deficient mice. Glycobiology 20:485–497
31. Mendoza R, Moody E, Enriquez M, Mejia S, Thordarson G (2011) Tumorigenicity of MCF-7 human breast cancer cells lacking the p38α mitogen-activated protein kinase. J Endocrinol 208:11–19
32. Hsu Y, Meng X, Ou L, Ip M (2010) Activation of the AMP-activated protein kinase-p38 MAP kinase pathway mediates apoptosis induced by conjugated linoleic acid in p53-mutant mouse mammary tumor cells. Cell Signal 22:590–599
33. Hui L, Bakiri L, Stepniak E, Wagner E (2007) P38 alpha: a suppressor of cell proliferation and tumorigenesis. Cell Cycle 6: 2429–2433
34. Hui L, Bakiri L, Mairhorfer A et al (2007) P38 alpha suppresses normal and cancer cell proliferation by antagonizing the JNK-c-Jun pathway. Nat Genet 39:741–749
35. McMullen M, Bryant P, Glembotski C, Vincent P, Pumiglia K (2005) Activation of p38 has opposing effects on the proliferation and migration of endothelial cells. J Biol Chem 280:20995–21003
36. Issbrücker K, Marti H, Hippenstiel S (2003) p38 MAP kinase—a molecular switch between VEGF-induced angiogenesis and vascular permeability. FASEB J 17:262–264
37. Luttun A, Brusselmans K, Fukao H et al (2002) Loss of placental growth factor protects mice against vascular permeability in pathological conditions. Biochem Biophys Res Commun 295: 428–434
38. Vetter M, Blumenthal S, Lindemann R (2005) Ets1 is an effector of protein kinase Cα in cancer cells. Oncogene 24:650–661